MITSUBISHI ELECTRIC RESEARCH LABORATORIES
https://www.merl.com

Fingerprinting-Based Outdoor Localization with 28-GHz Channel Measurement: A Field Study

Sun, Haijian; Wang, Pu; Pajovic, Milutin; Koike-Akino, Toshiaki; Orlik, Philip V.; Taira, Akinori; Nakagawa, Kenji

TR2020-056 May 13, 2020

Abstract

This paper considers localization with 28-GHz millimeter wave (mmWave) channel measurements in an outdoor environment. Compared with mmWave channel characterization by real-world experiments, localization using real-world 28-GHz experiments has been much less reported. To fill the gap, we report here a preliminary field study of using real-world 28-GHz channel frequency responses (CFR) with a wide bandwidth of 500 MHz for outdoor localization. Specifically, we employ a fingerprinting-based localization approach by registering the location information using multiple wideband CFR measurements and exploring the transmit-receive antenna polarization. Our experimental results demonstrate that, with a full bandwidth of 500 MHz, a correlation-based fingerprinting localization can fully identify all 8 locations with a 1-m separation without any error. The probability of successful localization reduces to 97% or 91.5%, respectively, when two or just one narrowband (< 15 MHz) CFR measurements are used for the training dataset.

IEEE International Workshop on Signal Processing Advances in Wireless Communications (SPAWC)

Mitsubishi Electric Research Laboratories, Inc.
201 Broadway, Cambridge, Massachusetts 02139

Fingerprinting-Based Outdoor Localization with 28-GHz Channel Measurement: A Field Study

Haijian Sun*, Pu Wang, Milutin Pajovic, Toshiaki Koike-Akino, Philip V. Orlik
Mitsubishi Electric Research Laboratories (MERL)
Cambridge, MA 02139, USA

Akinori Taira, Kenji Nakagawa
Mitsubishi Electric Information Technology R&D Center
5-1-1, Ofuna, Kamakura City, 247-8501, Japan

***Abstract*—This paper considers localization with 28-GHz millimeter wave (mmWave) channel measurements in an outdoor environment. Compared with mmWave channel characterization by real-world experiments, localization using real-world 28-GHz experiments has been much less reported. To fill the gap, we report here a preliminary field study of using real-world 28-GHz channel frequency responses (CFR) with a wide bandwidth of 500 MHz for outdoor localization. Specifically, we employ a fingerprinting-based localization approach by registering the location information using multiple wideband CFR measurements and exploring the transmit-receive antenna polarization. Our experimental results demonstrate that, with a full bandwidth of 500 MHz, a correlation-based fingerprinting localization can fully identify all 8 locations with a 1-m separation without any error. The probability of successful localization reduces to 97% or 91.5%, respectively, when two or just one narrowband (< 15 MHz) CFR measurements are used for the training dataset.**

I. Introduction

Leveraging a large number of antennas and RF chains to support many single-/multiple-antenna users at high-frequency millimeter wave (mmWave) bands, next-generation (5G) base stations and WiFi can significantly increase the spectral efficiency and provide high spatial beamforming resolution [1], [2]. More specifically, it can mitigate propagation loss by exploiting large array gain due to coherent beamforming/combining, reduce interference-leakage as channel estimation errors vanish asymptotically in the large-dimensional vector space, simplify signal processing algorithms, and reduce inter-user interference with high beamforming resolution.

Despite all these benefits, new challenges exist for system design and hardware implementation. For example, hardware cost and power consumption become prohibitively high when the number of RF chains is large and high-resolution analog-to-digital converters (ADCs) are employed. To meet these challenges, several transceiver architectures have been proposed. One is a hybrid analog/digital architecture that can reduce the number of RF chains by combining subarrays of antennas with switches, phase shifters and lenses, followed by digital sampling of the combined signals [3]–[5]. With more degrees of freedom, a hybrid precoder can support multi-stream transmission, while keeping the system cost, complexity, and power consumption low. Another one is a fully digital architecture with low-resolution ADCs [6], [7].

While the majority of 5G research activities are dedicated to data communication, the exploration of upcoming 5G mmWave signals for localization has received rising attention over the past few years. The mmWave localization may be more technically and commercially appealing when miniature 5G infrastructures are massively deployed in both indoor and outdoor environments hence seamless indoor and outdoor localization becomes more feasible for connected cars, robots, drones, and other mobile users. Its applications in Internet of Things (IoT), machine-to-machine (M2M) communications in factory automation, and smart buildings (logistics and smart mobility) are also highly anticipated.

The advantages of mmWave signals for localization come from the fact that a higher temporal resolution can be achieved due to the larger bandwidth, higher spatial directivity [8]–[10], and limited scattering [11]. In [12], *Shahmansoori et. al* proposed a three-stage position and orientation estimation method based on generated mmWave signals. A direct localization technique for massive MIMO based on AoA and TOA was proposed in [13]. It considered both line-of-sight (LOS) and non-line-of-sight (NLOS) impacts. Furthermore, *Lin et. al* investigated 3-D indoor mmWave localization using a large-scale uniform cylindrical array [14]. They reduced the reflection and scattering components with channel compression techniques.

In terms of the localization algorithms, fingerprinting and triangulation are two dominant techniques for RF-based localization systems. The former approach exploits location-specific signatures of each position. Typically, it involves two stages. In the first stage, a data collection of each location is required, the data then will be stored for future comparison with the second phase where the online data is collected. Earlier efforts have investigated the performance of fingerprinting-based techniques using received signal strength indicator (RSSI) [15] and full channel state information (CSI) at sub-6 GHz bands [16], [17]. On the other hand, triangulation utilizes the geometric property by pinpointing the location of interest with triangle calculations.

*H. Sun is with the department of Computer Science, University of Wisconsin-Whitewater, Whitewater, WI, 53190. The work was performed when H. Sun was an intern at MERL.

Compared with existing efforts on the mmWave outdoor localization using synthetic data, this paper introduces the first step of a series of real-world field studies using 28-GHz mmWave signals for both indoor and outdoor localization applications. Here we report our analysis results for an outdoor environment applying the fingerprinting approach with wideband channel frequency response (CFR) measurements as location-specific signatures. Our experimental results demonstrate that, with a full bandwidth of 500 MHz, a correlation-based fingerprinting localization can fully identify all 8 locations with a 1-m separation without any error. The probability of successful localization reduces to 97% or 91.5%, respectively, when two or just one narrowband (< 15 MHz) CFR measurements are used for the training dataset.

The remainder of the paper is organized as follows. In Section II, we introduce a correlation-based fingerprinting location algorithm by using the CFR measurements. Section III discusses the 28-GHz mmWave measurement system. Section IV describes the creation of training and test datasets. Performance evaluation is shown in Section V followed by Conclusions.

II. Localization using mmWave Infrastructure

In this section, we introduce the correlation-based fingerprinting localization algorithm which was used extensively in indoor localization. In Section V, we will also use it to analyze our 28-GHz channel measurements in an outdoor environment. Since we collect the channel state information (CSI) or, equivalently, channel frequency response (CFR), the CFR is used as location-specific fingerprints.

Given two CFR vectors $\mathbf{h}$ and $\mathbf{h}'$, the normalized cross correlation criterion computes

$$\gamma_{\text{CFR}}(\mathbf{h}, \mathbf{h}') = \frac{|\mathbf{h}^H \mathbf{h}'|^2}{\|\mathbf{h}\|_2 \|\mathbf{h}^{(l)}\|_2}, \tag{1}$$

where $(\cdot)^H$ denotes the Hermitian (complex transpose) operator and $\|\cdot\|_2$ is the ℓ_2 norma of a vector. Here, we define the CFR vector over multiple dimensions. In practice, the collected CFR can be a function of (frequency) subcarriers, transmit-receive polarization, transmitting beams, *et al*. This results in a multi-dimensional CFR datacube. To compute the normalized cross-correlation, we first vectorize the multi-dimensional CFR datacube into corresponding CFR vectors and then feed the vectors into (1).

For the correlation-based fingerprinting localization, one usually collects the training dataset at a set of known locations. This preliminary research collects a total of training dataset for L locations-of-interest. For a given location, $R \geq 1$ realizations of CFR measurements (usually taken at a different time) are stored. Overall, we have a training dataset of $R \times L$ CFRs for L known locations.

When new CFR measurements $\tilde{\mathbf{h}}$ from an unknown location are available, the problem of localization can be cast into an multi-hypothesis testing problem as follows

$$\hat{l} = \arg \max_{\substack{r=1,\cdots,R \\ l=1,\cdots,L}} \gamma_{\text{CFR}}(\mathbf{h}^{(r)}(l), \tilde{\mathbf{h}}). \tag{2}$$

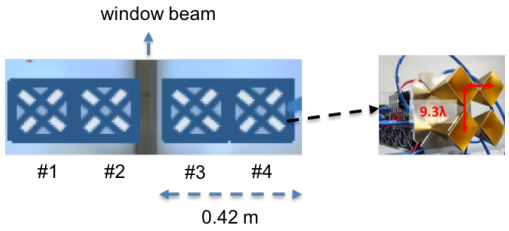

Fig. 1. A multi-beam transmitter supported by 4 sets of 2×2 rectangular horn antennas at 28 GHz.

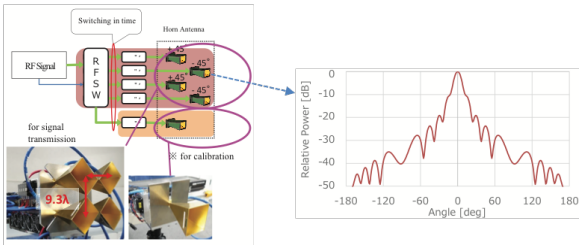

Fig. 2. Each set of 2×2 horn antennas is switched in time for data transmission.

For a candidate location, we first compute the cross correlation γ_{CFR} between each of the R realizations $\mathbf{h}^{(r)}(l)$ and the new CFR measurement $\tilde{\mathbf{h}}$. Then, for that candidate location, the largest one from the R cross correlation values (in other words, identify the most similar fingerprint feature from R realizations) is saved. We iterate the above computation over all L candidate locations and declare the location as the one giving the maximum cross-correlation value.

In practice, an additional step of comparing the maximum cross-correlation value with a pre-determined threshold is implemented to efficiently reduce the probability of false alarm. This is equivalent to expanding the multi-hypothesis testing problem of (2) by adding a null hypothesis $\mathcal{H}_0$

$$\gamma_l = \arg \max_{r=1,\cdots,R} \gamma_{\text{CFR}}(\mathbf{h}^{(r)}(l), \tilde{\mathbf{h}}) \tag{3}$$

$$\hat{l} = \begin{cases} \arg\max_{l=1,\cdots,L} \gamma_l, & \text{if } \max_{l=1,\cdots,L} \gamma_l \geq \Gamma \\ \text{excluded from } L \text{ locations}, & \text{otherwise} \end{cases}$$

where Γ is a proper threshold to be selected for a given probability of false alarm. In our experiment, we only implement the multi-hypothesis testing of (2) since the new CFR measurement $\tilde{\mathbf{h}}$ is always taken from one of L locations in the fingerprinting dataset.

III. Experiment Setting

To collect the 28-GHz channel measurement, probing signals are generated using a vector signal generator with a wide carrier frequency range. The carrier frequency was set to 27.89 GHz and the bandwidth is 500 MHz. The generated signal is amplified before feeding into horn antennas for channel sounding. At the receiver side, a broadband digital processing receiver is used to obtain the I/Q channel measurement for subsequent data analysis.

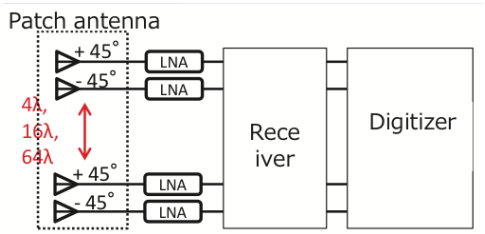

Fig. 3. The system architecture for the receiver side.

A. Transmitter Architecture

The transmitter side consists of 4 sets of 2×2 horn antennas to simulate a multi-stream hybrid beamforming, as shown in Fig. 1. The combined lateral length of the left two (#1 and #2) or right two sets (#3 and #4) is 0.42 m with a window beam in the middle. This setting is used to form 4 azimuth beams at 4 directions at $\{-9°, -3°, 3°, 9°\}$, respectively.

Within each set, the 2×2 horn antennas are arranged in an **X** shape to excite 2 polarization directions at $+45°$ and $-45°$, respectively. They are separated with a horizontal and vertical distance of 9.3λ, where λ denotes the corresponding wavelength. To enable data transmission from each horn antenna, we used an RF switcher to connect the signal generator to one horn antenna at a time. Fig. 2 shows the RF architecture with an RF switcher (RFSW). For the calibration purpose, one additional horn antenna is used. Each individual horn antenna has an antenna gain of 24 dBi with a one-side 3-dB beamwidth of 6°, as shown in the right plot of Fig. 2. The effective isotropic radiated power (EIRP) is 39.3 dBm. Overall, this architecture simulates a 16-stream (4×4) multiplexing scheme with 4 streams pointing at the same azimuth direction with different polarizations.

The probing signal is generated by a signal generator as a chirp signal with a bandwidth of 500 MHz at the center frequency of 27.89 GHz. Specifically, a triangular (up/down) sweeping pattern is used for the chirp generation. Each chirp duration (burst length) is about 11.1 μs with a coherent processing interval (burst interval) of 13.3 μs.

B. Receiver Architecture

At the receiver side, the system architecture is shown in Fig. 3. Polarized patch antennas are used to receive the transmitted signal. Then the received signal passes through a low noise amplifier (LNA) before the digital sampling. After the digitalization, we can obtain channel measurements at 6400 subcarriers with a subcarrier interval of 75 kHz around the center frequency of 27.89 GHz. The pair of patch antennas is arranged vertically with a polarization direction at $+45°$ at the top and the other at $-45°$ at the bottom. For both polarization directions, the azimuth beampattern is relatively flat to cover wide azimuthal angles, as shown in Fig. 4. Even though they are not visually distinct, the cross-polar discrimination (XPD) is about 10 dB.

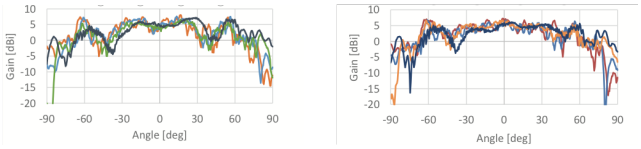

(a) (b)

Fig. 4. Patch antenna beampatterns for a) $+45°$ polarization at the left; and b) $-45°$ polarization at the right.

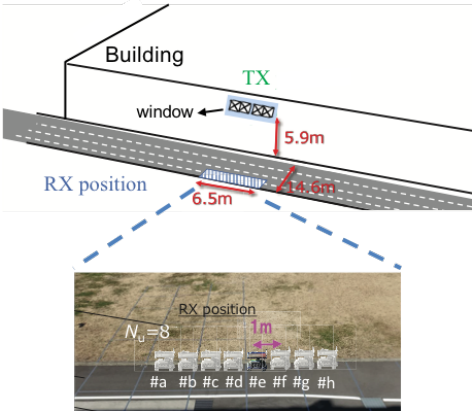

Fig. 5. Experiment setting for an outdoor environment.

C. Experiment Settings

The data collection was conducted in an outdoor environment with a common road outside a building. The transmitter is placed through a window at the building with a height of 5.9 m above the road level. The receiver is placed around the dashed area at the outer lane of the road. The ground-level distance between the transmitter and receiver is about 14.6 m. We moved the receiver station to 8 different locations (labeled from $\#a$ to $\#h$ as shown in Fig. 5) with a separation of 1 m. For each location, we only recorded *one-snapshot* the channel measurement corresponding to 16 transmitting horn antennas and 4 receiving patch antennas.

IV. Creating Training and Test Datasets

In real-world experiments, collected measurements may be scarce due to resource limitations. In our experiment, only one-realization channel measurement was recorded for each location. As a result, we cannot have both training and test datasets. In other words, we need at least 2 realizations for each location, one for the training dataset and one for the test dataset, to analyze the fingerprinting-based localization performance. To overcome this challenge, we explore the *transmit-receive polarization* to create multiple virtual realizations for a given location and then split these virtual realizations into the training and test datasets.

By numbering the transmit horn antennas and receive patch antennas in Fig. 6, we can have 16 transmit-receive polarization pairs for one location. From these 16 pairs, we observed that certain pairs show similar CFR patterns due to their transmit-receive polarization. For instance, the upper left plot of Fig. 7 shows four CFR curves corresponding

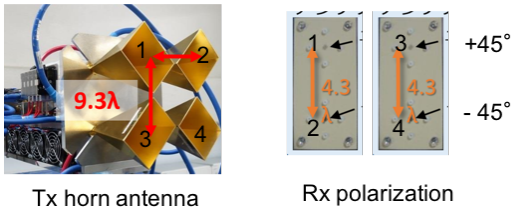

Fig. 6. Exploring transmit-receive polarizations to create multiple virtual realizations for each location.

to four polarization pairs: $\{1,1\}$, $\{1,3\}$, $\{4,1\}$ and $\{4,3\}$ where the first number denotes the horn antenna index and the second number is the patch antenna index. It is noted that the four CFR curves are similar to each other, up to a shift of frequency dips (or, equivalently, a delay in the time domain). This observation aligns well with the physical implications of the transmit-receive polarization in Fig. 6. That is, the horn antennas 1 and 4 have the same transmitting polarization at $-45°$, while the patch antennas 1 and 3 share the same receiving polarization at $+45°$. As a result, we can treat the 4 CFR measurements from the four polarization pairs as 4 virtual realizations for the same location. In other words, we can treat these four CFR measurements taken from one fixed transmit-receive antenna pair at four different time instants.

Similarly, we can find other transmit-receive polarization pairs sharing similar CFR measurements. Therefore, for a given location l, we can divide the one-realization experimental measurement into M virtual realizations. Specifically, we create $M = 4$ realizations by splitting similar transmit-receive polarization pairs into different realizations. One choice is listed as follows:

$$\begin{aligned}
&\text{Realization 1: } \{1,1\},\{2,1\},\{1,2\},\{2,2\},\\
&\text{Realization 2: } \{4,1\},\{3,1\},\{4,2\},\{3,2\},\\
&\text{Realization 3: } \{1,3\},\{2,3\},\{1,4\},\{2,4\},\\
&\text{Realization 4: } \{4,3\},\{3,3\},\{4,4\},\{3,4\}.
\end{aligned} \tag{4}$$

Other choices are possible by permutations of similar transmit-receive pairs into different realizations. Once we fix the choice of realizations, we apply the same rule to all L locations to create M realizations for all locations. To further explore the difference in traveling distances, we may have $M = 8$ virtual realizations for the fingerprinting dataset.

With a total of virtual $L \times M$ realizations, we can allocate R realizations into the training dataset and $M - R$ realizations to the test dataset for each location. This allocation will be used to evaluate the fingerprinting-based localization performance.

V. Performance Evaluation

In this section, we present our results for the fingerprinting-based mmWave localization system. As mentioned in the above section, the one-realization measurement is divided into either $M = 4$ or $M = 8$ virtual realizations for the fingerprinting dataset.

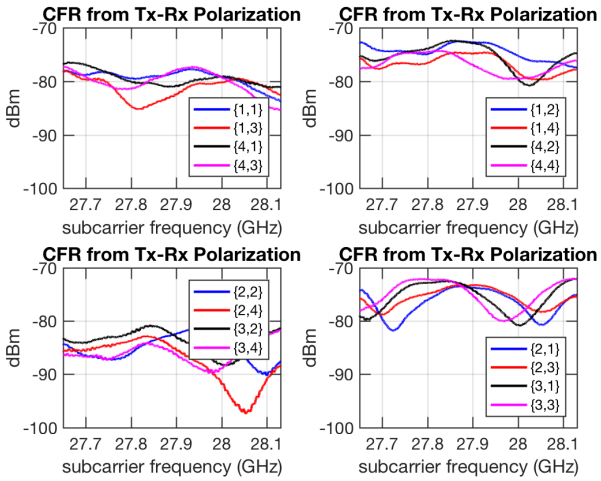

Fig. 7. Channel frequency responses for 16 transmit-receive polarization pairs. The first number in the bracket denotes the transmit horn antenna while the second number denotes the receive patch antenna.

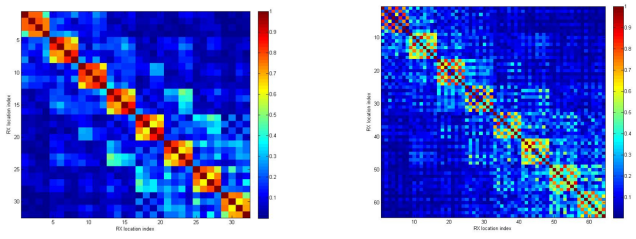

(a) (b)

Fig. 8. Confusion matrices for a) $M = 4$ realizations and b) $M = 8$ realizations.

We first assess the separation distance between different locations l and different realizations r. For this purpose, we use the confusion matrix defined as

$$\mathbf{C}(i,j) = \gamma_{\text{CFR}}(\mathbf{h}^{(r_1)}(l_1), \mathbf{h}^{(r_2)}(l_2)) \tag{5}$$

where $i = (l_1 - 1) \times L + r_l$, $j = (l_2 - 1) \times L + r_2$, and $\gamma_{\text{CFR}}(\cdot,\cdot)$ denotes the normalized cross correlation of (1). With $M = 4$, Fig. 8 (a) shows the computed confusion matrix over $L = 8$ locations and $M = 4$ realizations which yields a 32×32 matrix. It is easy to notice its dominant block-diagonal structure with a size of 4×4. These 4×4 diagonal blocks essentially imply strong similarities among the $R = 4$ virtual realizations we created from the transmit-receive polarization pairs. Moreover, small off-diagonal blocks of the confusion matrix exhibit these fingerprinting dataset preserves well the location-specific features. With $M = 8$, Fig. 8 (b) shows the confusion matrix for all $L = 8$ locations and $M = 8$ realizations. One can still notice the block-diagonal structure but it is less dominant than the $M = 4$ counterpart.

Next we split the M virtual realizations for each location into R realizations for training and $(M - R)$ for testing. A localization is considered to be successful if the correlation-based fingerprinting scheme declares the true location (out of $L = 8$ locations). Then the probability of successful

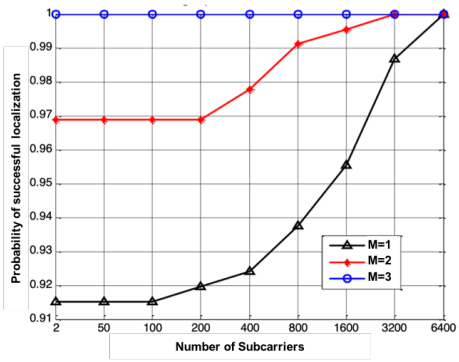

Fig. 9. Probability of successful localizations as a function of subcarriers.

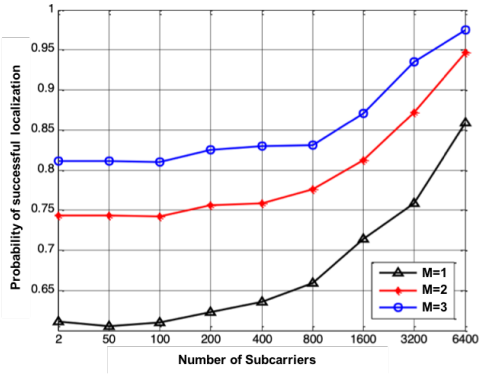

Fig. 10. 1-m localization accuracy as a function of the number of subcarriers under eight groups of datasets with varying training indices.

localization is defined as the ratio of the number of successful localization to the total number of tests.

Fig. 9 shows the probability of successful localization as a function of the number of subcarriers when, out of $M = 4$ virtual realizations, a) only $R = 1$ realization is used for training dataset at each location (black curves); b) $R = 2$ realizations are used for training dataset at each location (red curves); and 3) $R = 3$ realizations are used for training dataset at each location (blue curves). With more realizations in the training dataset, e.g., $R = 3$, the localization accuracy reaches to 100%, even with only two subcarriers. The accuracy decreases slightly when we use fewer realizations (smaller R) in the training set. Nevertheless, the accuracy can still reach 100% when all subcarriers are used for localization. The lowest probabilities of successful localization are around 97% for $R = 2$ and, respectively, 91.5% for $R = 1$ when the number of subcarriers is small.

Fig. 10 shows the probability of successful localization as a function of the number of subcarriers when we have $M = 8$ realizations. Similar to the case of $M = 4$, the performance improves as the number of subcarriers increases. The best probability of successful localization of 97% is attained with all 6400 subcarriers when $R = 3$. The best performance drops to 95% for $R = 2$ and around 85% for $R = 1$. Comparison between Fig. 10 and Fig. 9 shows that the choice of $M = 4$ of (4) yields better localization performance.

VI. Conclusions

Our outdoor experiment and data analysis demonstrated that, with a full transmit aperture and an effective bandwidth of 500 MHz, a simple correlation-based fingerprinting localization scheme can successfully identify all 8 locations with a 1-m separation without localization error. This preliminary analysis drives us to use a 28-GHz phased-array testbed (such as Mitsubishi Electric's hybrid phased-array RF module) for further data collection in various scenarios.

VII. Acknowledgements

This paper includes a part of the results of "The research and development project for realization of the fifth generation mobile communications system" commissioned by Japan's Ministry of Internal Affairs and Communications.

References

[1] Z. Pi and F. Khan, "An introduction to millimeter-wave mobile broadband systems," *IEEE Commun. Mag.*, vol. 49, no. 6, June 2011.

[2] A. Alkhateeb, O. E. Ayach, G. Leus, and R. W. Heath, Jr., "Channel estimation and hybrid precoding for millimeter wave cellular systems," *IEEE J. Sel. Topics. Signal Process.*, vol. 8, pp. 831-846, Oct. 2014.

[3] W. Roh et al., "Millimeter-wave beamforming as an enabling technology for 5G cellular communications: theoretical feasibility and prototype results," *IEEE Commun. Mag.*, vol. 52, no. 2, pp. 106-113, Feb 2014.

[4] R. W. Heath, N. Gonzalez-Prelcic, et. al., "An Overview of Signal Processing Techniques for Millimeter Wave MIMO Systems," *IEEE J. Sel. Topics Signal Process.*, vol. 10, Apr. 2016.

[5] A. Alkhateeb, G. Leus and R. W. Heath, "Limited Feedback Hybrid Precoding for Multi-User Millimeter Wave Systems," *IEEE Trans. Wireless Commun.*, vol. 14, no. 11, pp. 6481-6494, Nov. 2015.

[6] J. Mo, P. Schniter and R. W. Heath, "Channel Estimation in Broadband Millimeter Wave MIMO Systems With Few-Bit ADCs," *IEEE Trans. Signal Process.*, vol. 66, no. 5, pp. 1141-1154, Mar. 2018.

[7] J. Choi, B. L. Evans and A. Gatherer, "Resolution-Adaptive Hybrid MIMO Architectures for Millimeter Wave Communications," *IEEE Trans. Signal Process.*, vol. 65, no. 23, pp. 6201-6216, Dec. 2017.

[8] M. Pajovic, P. Wang, T. Koike-Akino, H. Sun, and P. Orlik, "Fingerprinting-Based Indoor Localization with Commercial MMWave WiFi - Part I: RSS and Beam Indices," in *GLOBECOM 2019*, Dec. 2019.

[9] P. Wang, M. Pajovic, T. Koike-Akino, H. Sun, and P. Orlik, "Fingerprinting-Based Indoor Localization with Commercial MMWave WiFi - Part II: Spatial Beam SNRs," in *GLOBECOM 2019*, Dec. 2019.

[10] T. Koike-Akino, P. Wang, M. Pajovic, H. Sun, and P. V. Orlik, "Fingerprinting-Based Indoor Localization with Commercial MMWave WiFi: A Deep Learning Approach," in *IEEE Access*, April 2020.

[11] M. Vari and D. Cassioli, "mmWaves RSSI indoor network localization," in *ICC 2014*, Sydney, NSW, Australia, Jun. 2014, pp. 127-132.

[12] A. Shamansoori, G. E. Garcia, G. Destino, et.al., "Position and orientation estimation through millimeter-wave MIMO in 5G systems", *IEEE Trans. Wireless Commun.,* vol. 17, pp. 1822-1835, Mar. 2018.

[13] N. Garcia, H. Wymeersch, E. G. Larsson, A. M. Haimovich, and M. Coulon, "Direct localization for massive MIMO," *IEEE Trans. Signal Process.*, vol. 65, no. 10, pp. 2475-2487, May 2017.

[14] Z. Lin, T. Lv, and P. T. Mathiopoulos, "3-D indoor positioning for millimeter-Wave massive MIMO systems", *IEEE Trans. Commun*, vol. 66, no. 6, Jun 2018.

[15] M. Youssef and A. Agrawala, "The Horus WLAN location determination system," in *Proc. 3rd Int. Conf. Mobile Syst. Appl. Services (MobiSys)*, Seattle, WA, USA, 2005, pp. 205218.

[16] X. Wang, L. Gao, S. Mao and S. Pandey, "CSI-Based Fingerprinting for Indoor Localization: A Deep Learning Approach," *IEEE Trans. Veh. Technol.*, vol. 66, no. 1, pp. 763-776, Jan. 2017.

[17] C. Chen, Y. Chen, Y. Han, H. Lai, F. Zhang and K. J. R. Liu, "Achieving centimeter-accuracy indoor localization on WiFi platforms: a multi-antenna approach," *IEEE Internet of Things Journal*, vol. 4, no. 1, pp. 122-134, Feb. 2017.